Bioconjugate Chemistry

pubs.acs.org/bc

Article

Tick Saliva Protein Evasin-3 Allows for Visualization of Inflammation in Arteries through Interactions with CXC-Type Chemokines Deposited on Activated Endothelium

Stepan S. Denisov, Alexandra C. A. Heinzmann, Tanja Vajen, Mark H. M. Vries, Remco T. A. Megens, Dennis Suylen, Rory R. Koenen, Mark J. Post, Johannes H. Ippel, Tilman M. Hackeng, and Ingrid Dijkgraaf*

Cite This: *Bioconjugate Chem.* 2020, 31, 948–955

Read Online

ACCESS | Metrics & More | Article Recommendations | Supporting Information

ABSTRACT: Atherosclerosis is one of the leading causes of mortality in developed and developing countries. The onset of atherosclerosis development is accompanied by overexpression of several inflammatory chemokines. Neutralization of these chemokines by chemokine-binding agents attenuates atherosclerosis progression. Here, we studied structural binding features of the tick protein Evasin-3 to chemokine (C-X-C motif) ligand **1** (CXCL1). We showed that Evasin-3-bound CXCL1 is unable to activate the CXCR2 receptor, but retains affinity to glycosaminoglycans. This observation was exploited to detect inflammation by visualizing a group of closely related CXC-type chemokines deposited on cell walls in human endothelial cells and murine carotid arteries by a fluorescent Evasin-3 conjugate. This work highlights the applicability of tick-derived chemokine-binding conjugates as a platform for the development of new agents for inflammation imaging.

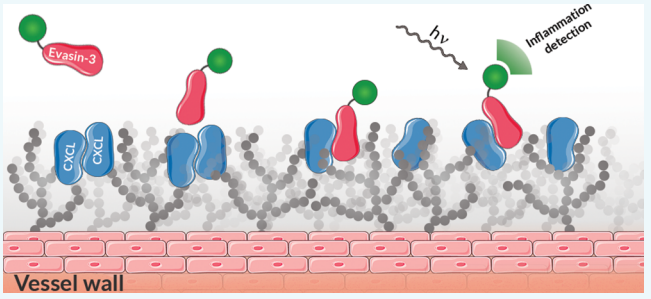

INTRODUCTION

Atherosclerosis is a chronic inflammatory disease characterized by accumulation of lipid-rich plaques in the wall of large or medium-sized arteries and is one of the leading causes of morbidity and mortality in developed countries.[1] Development of atherosclerotic lesions begins with adhesion of monocytes to endothelial cells (EC) caused by an elevated level of plasma cholesterol.[2] The underlying processes of monocyte adhesion are mediated by chemokines—small structurally conservative proteins[3]—which are presented on activated endothelium at the luminal surface of atherosclerotic arteries and regulate cell trafficking and recruitment.[4−6] The chemokine (C-X-C motif) ligand **1** (CXCL1, melanoma growth stimulatory activity (MGSA), GRO-α) is a major player in atherosclerosis development at early stages.[7] Therefore, neutralization of CXCL1 by chemokine-binding agents could be beneficial for reduction of atherosclerosis progression, as it has been proven for CCL17 and CCL5/CXCL4 heterodimer.[8,9]

Intervention in the chemokine signaling system and neutralization of chemokines are widely exploited by pathogenic organisms and parasites such as ticks to evade an immune response of their hosts.[10] Evasins are a group of small cysteine-rich chemokine-binding proteins produced in salivary glands of ticks.[11,12] Evasin-3 is of particular interest as it binds to several CXC-type chemokines including CXCL1[13] and has been shown to reduce neutrophilic inflammation in mouse models of carotid atherosclerosis and ischemic stroke.[14]

Here, anti-CXCL1 activity of Evasin-3 was investigated using chemotaxis assays and solution NMR spectroscopy. Based on obtained structural data, we showed that Evasin-3 does not block interactions of CXCL1 with glycosaminoglycans (GAGs) and thus could be used as an inflammation imaging agent. As a result, an Oregon Green 488 Evasin-3 conjugate was synthesized by solid-phase peptide synthesis (SPPS) and characterized by surface plasmon resonance (SPR) biosensor analysis. Subsequently, this conjugate was successfully applied for visualization of a group of closely related CXC-type chemokines in human microvascular endothelial cells and in activated endothelium of mounted whole mouse carotid arteries.

Received: February 18, 2020
Revised: February 20, 2020
Published: February 20, 2020

https://dx.doi.org/10.1021/acs.bioconjchem.0c00095
Bioconjugate Chem. 2020, 31, 948–955

RESULTS AND DISCUSSION

Monocyte arrest at early stages of atherosclerosis development is promoted through activation of CXCR2 receptor by CXCL1 deposited on heparan sulfate proteoglycans on the endothelial cell surface.[15,16] To investigate whether Evasin-3 could inhibit CXCL1-mediated monocyte adhesion, flow chamber adhesion assays with human umbilical vein endothelial cells (HUVECs) were performed. Endothelial cells were activated by lysophosphatidic acid (LPA) treatment, since it has been shown to trigger CXCL1 deposition on the cell surface.[5] Adhesion of monocyte to EC was significantly diminished in the presence of 10 nM Evasin-3, when compared with LPA-induced EC (Figure 1A). In addition to monocytes, neutrophils have a proatherogenic function in the initiation of atherosclerotic lesion formation.[17,18] Furthermore, symptomatic atherosclerotic plaques have a higher number of intraplaque neutrophils when compared with asymptomatic lesions, pointing to a pathogenic role of these leukocyte subtypes.[19] Evasin-3 dramatically reduced adhesion of neutrophils in the flow chamber assay compared with control LPA-activated endothelial cells (Figure 1B). The observed effect is in agreement with previously published data, showing that Evasin-3 inhibits neutrophil recruitment[20] and decreases neutrophil counts in carotid arteries.[14] However, LPA activation of ECs leads to increasing expression of not only CXCL1 but also CXCL8, CXCL6, CXCL3, and CXCL2 (Figure S1). Thus, observed monocyte and neutrophil adhesion inhibition is most likely the result of neutralization of multiple CXC-type chemokines by Evasin-3. To rule out the influence of other expressed CXC-type chemokines, a neutrophil chemotaxis assay was performed, in which CXCL1 deliberately was added as a chemoattractant. CXCL1-induced migration of neutrophils in these experiments was effectively inhibited by coincubation with 10 nM of Evasin-3 (Figure 1C,D).

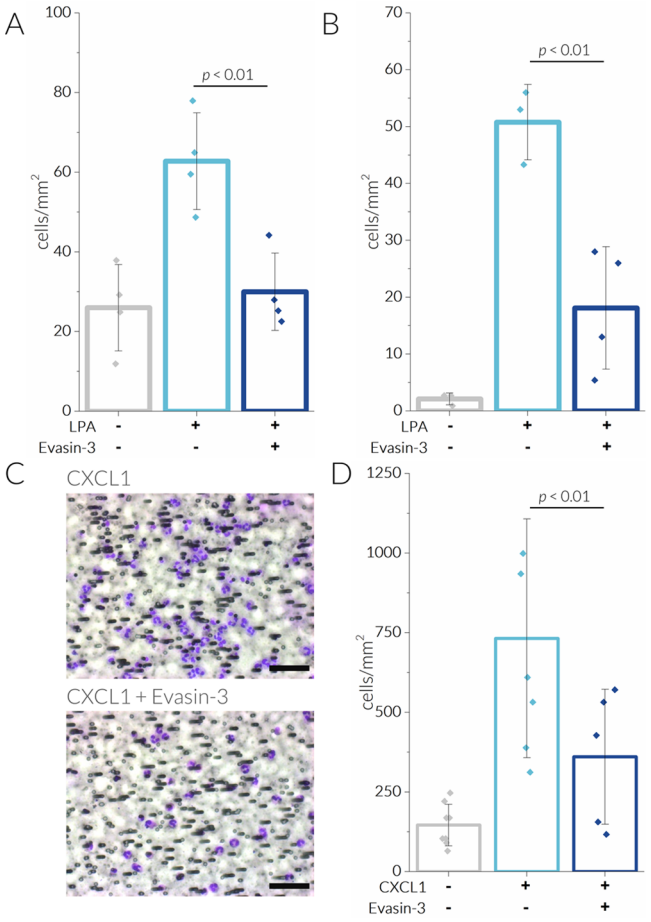

Figure 1. Evasin-3 inhibits migration and adhesion of monocytes and neutrophils. Influence of Evasin-3 on adhesion of monocytes (A) and neutrophils (B) to LPA activated HUVECs (n = 3−6). Data are represented as mean ± SD. C. Light microscopy images of 5 μm polycarbonate membrane after CXCL1-induced PMN migration in the absence (top) or presence (bottom) of Evasin-3. The poly lobular nuclei of PMNs are in purple; black dots represent the pores of the membrane. Scale bar is 50 μm. D. CXCL1-induced migration of monocytes in absence (n = 5) and presence of Evasin-3 (n = 5) compared with the control in the absence of chemoattractant (n = 8).

To shed light on the molecular basis of the anti-CXCL1 activity of Evasin-3, the formation of a CXCL1/Evasin-3 complex has been studied by NMR spectroscopy. In order to allow NMR experiments, CXCL1 and met-Evasin-3 (Evasin-3 variant with an N-terminal methionine) were obtained in uniformly ^{15}N- and ^{13}C-labeled forms. Then, sequential assignment was carried out for both unbound proteins and the CXCL1/met-Evasin-3 complex using a combination of 2D and 3D NMR spectra. Detailed analysis of NMR spectra of free [^{15}N, ^{13}C] met-Evasin-3 was published recently.[21] Addition of CXCL1 rapidly caused large changes in the ^{15}N−^{1}H HSQC spectrum with the most perturbed residues located in the F17−S21 and F38−G55 regions (Figure 2A and S2). In contrast, chemical shifts of the N- (L1−N16) and C-terminal (N56−R66) residues of met-Evasin-3 stayed unperturbed upon CXCL1 binding. To assess the influence of CXCL1 binding on N- and C-terminal regions, ^{15}N NOE relaxation values were measured to determine the local flexibility of the peptide chain (Figure 2B). Negative values for L1−D12 and V63−R66 regions indicate that N- and C-terminal regions stay flexible in both the free [^{15}N, ^{13}C] met-Evasin-3 and the CXCL1/[^{15}N, ^{13}C] met-Evasin-3 complex. These observations are in line with the previous reports observing that the Evasin-3 core region plays a crucial role in the chemokine binding, whereas the N- and C-termini do not participate in binding and remain flexible.[13,21]

A similar set of NMR spectra were recorded for [^{15}N, ^{13}C] CXCL1 in the free and in the met-Evasin3-bound form. These NMR data indicated the presence of the dimeric and monomeric forms of CXCL1 in a ∼1:1 ratio at a protein concentration of 50 μM (Figure 3A). The chemical shift perturbation (CSP) pattern of the monomer/dimer equilibria (Figure, 3C, top) shows that most affected CXCL1 residues are located in the β1-strand (S25−S30) and α-helix (K60, I62−N68), which comprise the intermolecular dimerization interface in the CXCL1 homodimer. Although perturbed residues in the N-loop (Q16−I18) and β2-strand (T38−T43) do not directly participate in the formation of the dimer interface; perturbation in this region could be explained by the indirect effect due to loss of steric interactions between the N-loop and the α-helix and disruption of the β1−β1 β-sheet upon CXCL1 dimer disruption, respectively. Addition of a slight excess of met-Evasin-3 to 50 μM [^{15}N,^{13}C] CXCL1 caused immediate changes in CXCL1 chemical shifts and resulted in the single set of NMR resonance signals indicating formation of 1:1 [^{15}N,^{13}C] CXCL1/met-Evasin-3 complex (Figure 3B). met-Evasin-3-induced CSP for monomeric CXCL1 are strictly

https://dx.doi.org/10.1021/acs.bioconjchem.0c00095
Bioconjugate Chem. 2020, 31, 948−955

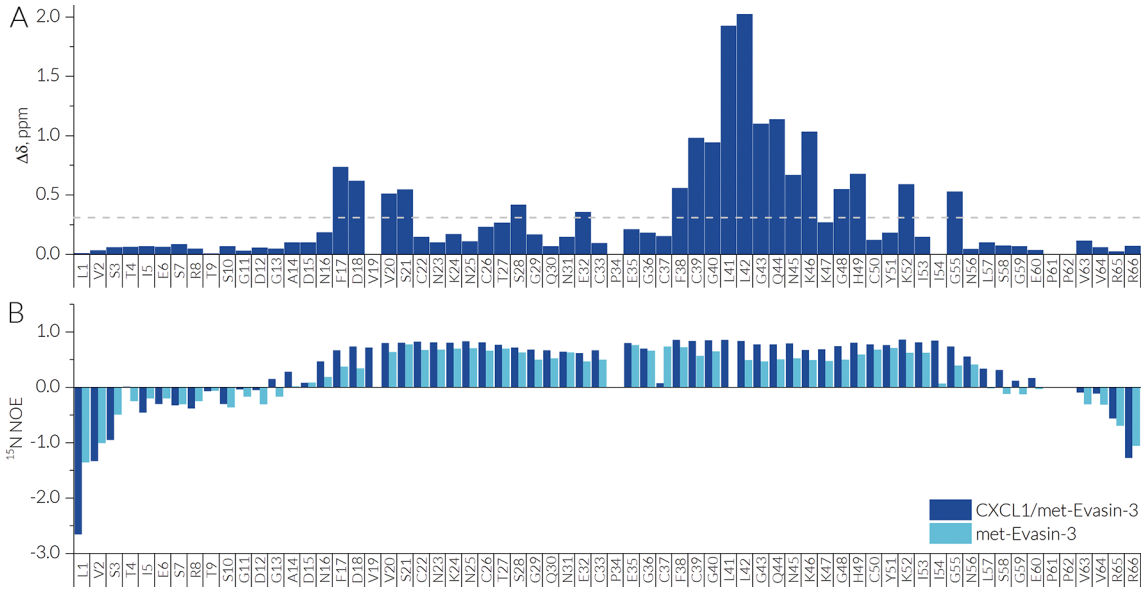

Figure 2. A. Chemical perturbation plot of 350 μM [^{15}N, ^{13}C] met-Evasin-3 upon binding of CXCL1 at 37 °C, pH 4.5. Delta values are expressed as the sum of weighted square roots of ^{1}H and ^{15}N chemical shifts perturbations; the dashed line indicates an average value of chemical shift perturbation. B. ^{15}N heteronuclear NOE relaxation values of 350 μM [^{15}N, ^{13}C] met-Evasin-3 in free form (light blue) and in the CXCL1/[^{15}N,^{13}C] met-Evasin-3 complex (dark blue).

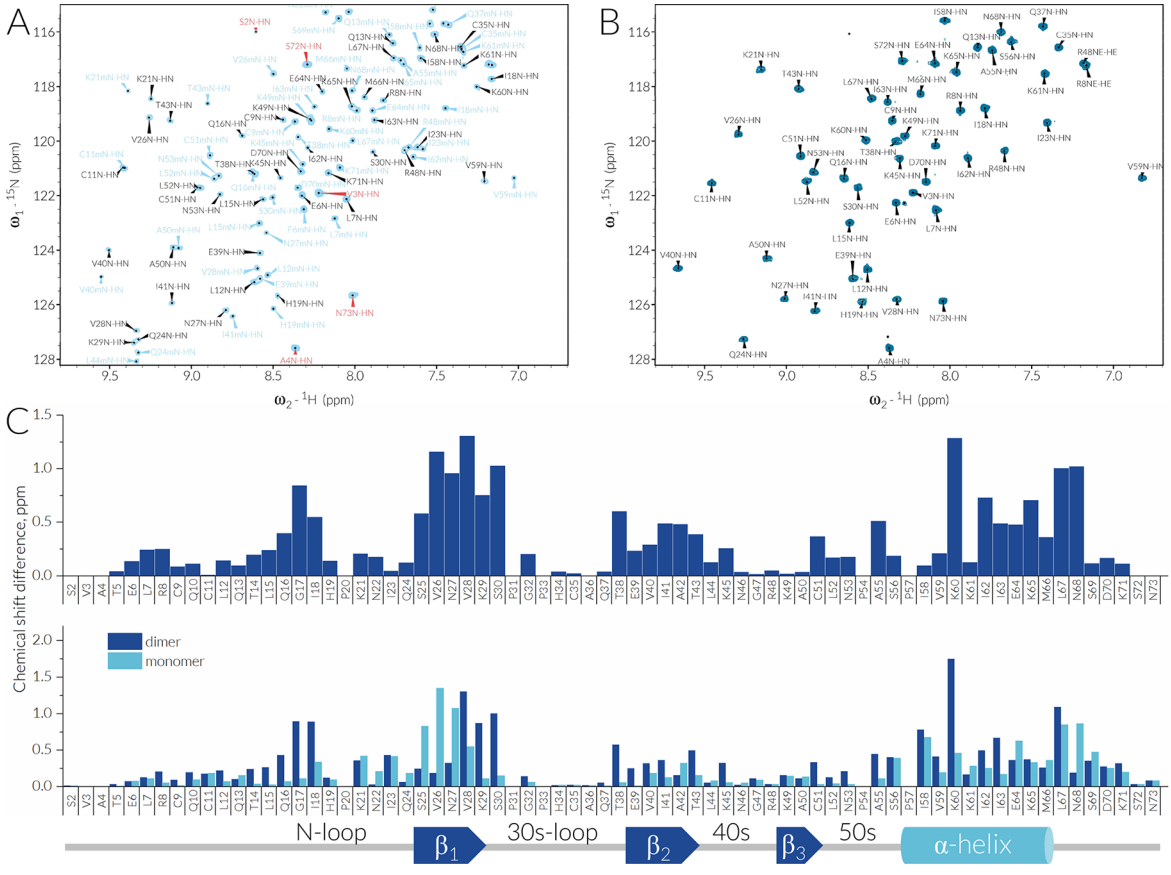

Figure 3. Binding of Evasin-3 disrupts CXCL1 dimer. ^{15}N−^{1}H HSQC spectrum of 50 μM [^{15}N, ^{13}C] CXCL1 (A) and ^{15}N−^{1}H HSQC spectrum of 50 μM [^{15}N, ^{13}C] CXCL1/met-Evasin-3 complex (B) at 37 °C, pH 4.5. Amide peaks of the monomeric form are labeled in blue; the dimeric form is in black; overlapping peaks are in red. Assignments of Asn, Gln, and Arg side chain peaks are hidden for clarity. C. Chemical shift perturbation plots for CXCL1 monomer/dimer equilibria (top), and upon met-Evasin-3 binding to CXCL1 (bottom). Delta values are expressed as the sum of weighted square roots of ^{1}H and ^{15}N chemical shift perturbations. The secondary structure of CXCL1 is derived from the crystal structure (PDB ID 1MGS).

https://dx.doi.org/10.1021/acs.bioconjchem.0c00095
Bioconjugate Chem. 2020, 31, 948−955

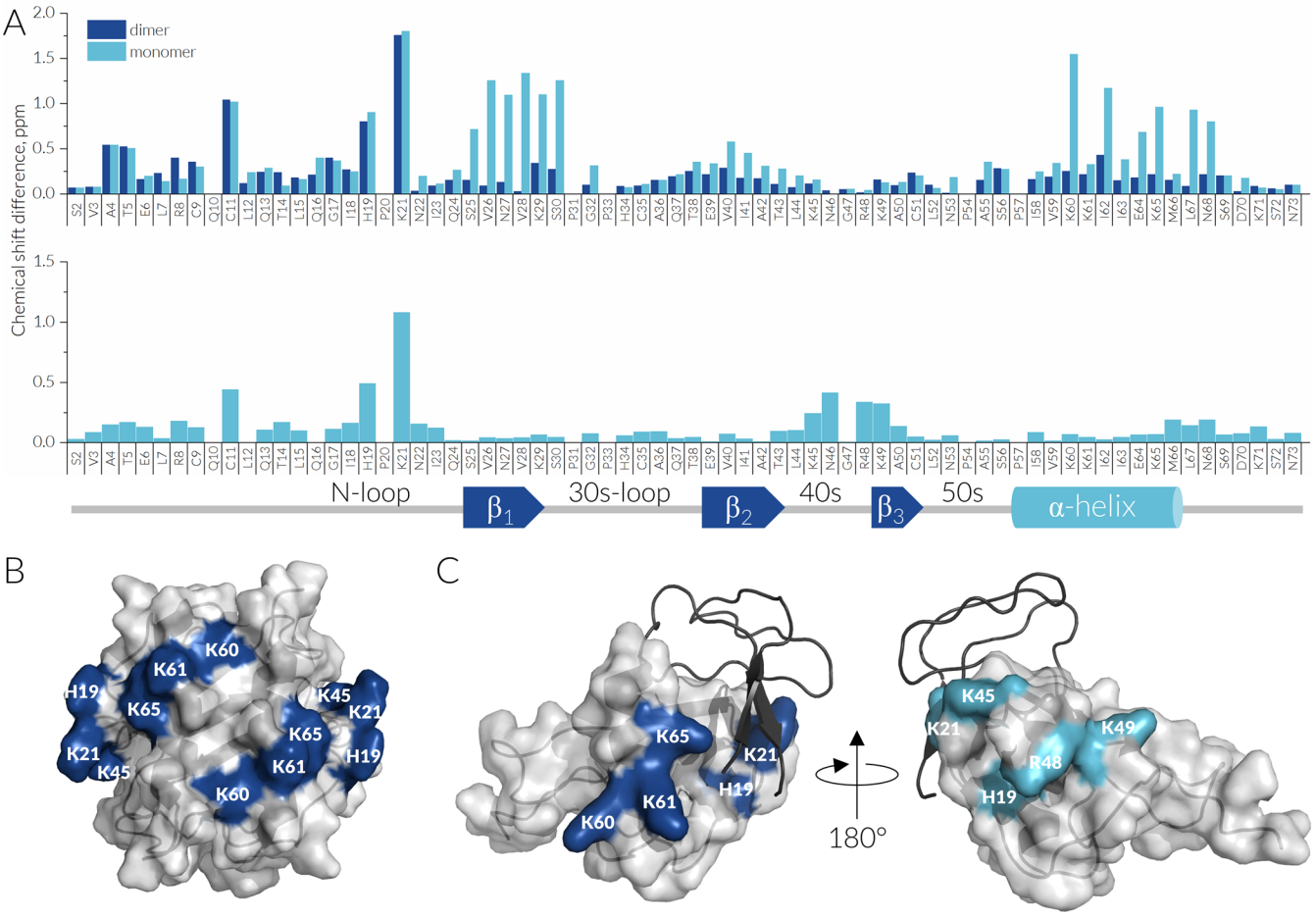

Figure 4. Binding of GAGs to CXCL1. A. Chemical shift perturbation plot of 250 μM [^{15}N, ^{13}C] CXCL1 (top) and 200 μM [^{15}N, ^{13}C] CXCL1/met-Evasin-3 (bottom) upon binding of Fondaparinux (Arixtra, GSK). B. GAG binding surface of the α-domain of CXCL1 dimer. C. α-Domain and positively charged residues of CXCL1 perturbed upon Fondaparinux binding depicted in the schematic representation of CXCL1/met-Evasin-3 complex. The representation is based on CXCL8/Evasin-3 complex; Evasin-3 is depicted in black serpentine; N- and C-termini are hidden for visibility.

located in two regions: β1-strand (S25−V28) and α-helix region (I58, E64, L67, N68), indicating the CXCL1/met-Evasin-3 complex interface (Figure 3C, bottom). The CSP pattern for Evasin-3 binding to the CXCL1 dimer mirrors the plot of CXCL1 dimerization with perturbations located in the N-loop (Q16−I18), β1-strand (V28, K29, S30), β2-strand (T38−T43), and α-helix (I58, K60, I62, I63, L67) regions. These perturbations follow the similar pattern observed for the CXCL8 dimer[21] and indicate disruption of the CXCL1 dimer upon binding of met-Evasin-3.

It has been shown that met-Evasin-3 binding effectively disrupts the interaction of CXCL8 with GAGs by intercalating in between the α-helix and the N-loop.[21] Although positively charged residues of the α-helix and the N-loop of CXCL1 participate in GAG binding similarly as in CXCL8, CXCL1 possesses more complex GAG binding topology having two non-overlapping α and β GAG binding domains.[22−24] To assess the structural relationships between the CXCL1/met-Evasin-3 complex and GAGs, binding of a synthetic heparin mimic—Fondaparinux (Arixtra, GSK)—to CXCL1 in the free and bound-by-met-Evasin-3 form was studied. Addition of 5-fold excess of Fondaparinux to 250 μM [^{15}N,^{13}C] CXCL1 led to a large chemical shift of both monomeric and dimeric CXCL1 and resulted in a single set of NMR signals (Figure S3). The CPS plot for the CXCL1 monomer indicates that Fondaparinux binding causes CXCL1 dimerization as residues of the β1-, β2-strands and α-helix are to a large extent perturbed (Figure 4A). Residues of N-terminus (A4, T5, C11) and N-loop (H19, K21) are substantially affected upon binding of GAG when compared to both free mono- and dimeric CXCL1. Large perturbations of H19 and K21 could indicate that binding of GAG is mediated mostly by the α-domain of CXCL1 (Figure 4B), as residues K45−R49, which constitute the β-domain, are not affected by addition of Fondaparinux.

GAG-induced CPS pattern for 200 μM of [^{15}N, ^{13}C] CXCL1/met-Evasin-3 complex largely diverts from the one for free di- and monomeric CXCL1 (Figure, 4A, bottom; Figure S4). Whereas H19 and K21 of the α-domain are affected similarly as in GAG binding to free CXCL1, unaffected residues of the β-domain in the free form (K45, R48, and K49) are substantially perturbed in the case of CXCL1/met-Evasin-3 complex. Changes in GAG binding mode could be explained by disruption of the CXCL1 dimer and therefore the GAG binding α-domain upon Evasin-3 binding (Figure 4C). As the integrity of the α-domain is lost in the CXCL1/Evasin-3 complex, binding of GAGs is reoriented toward residues from the α-domain (H19, K21) and β-domain (K45, R48, and K49), which represents a continuous positively charged surface (Figure 4D). The similar GAG binding plasticity was observed in the case of binding several GAG types to CXCL1.[25] This

https://dx.doi.org/10.1021/acs.bioconjchem.0c00095
Bioconjugate Chem. 2020, 31, 948−955

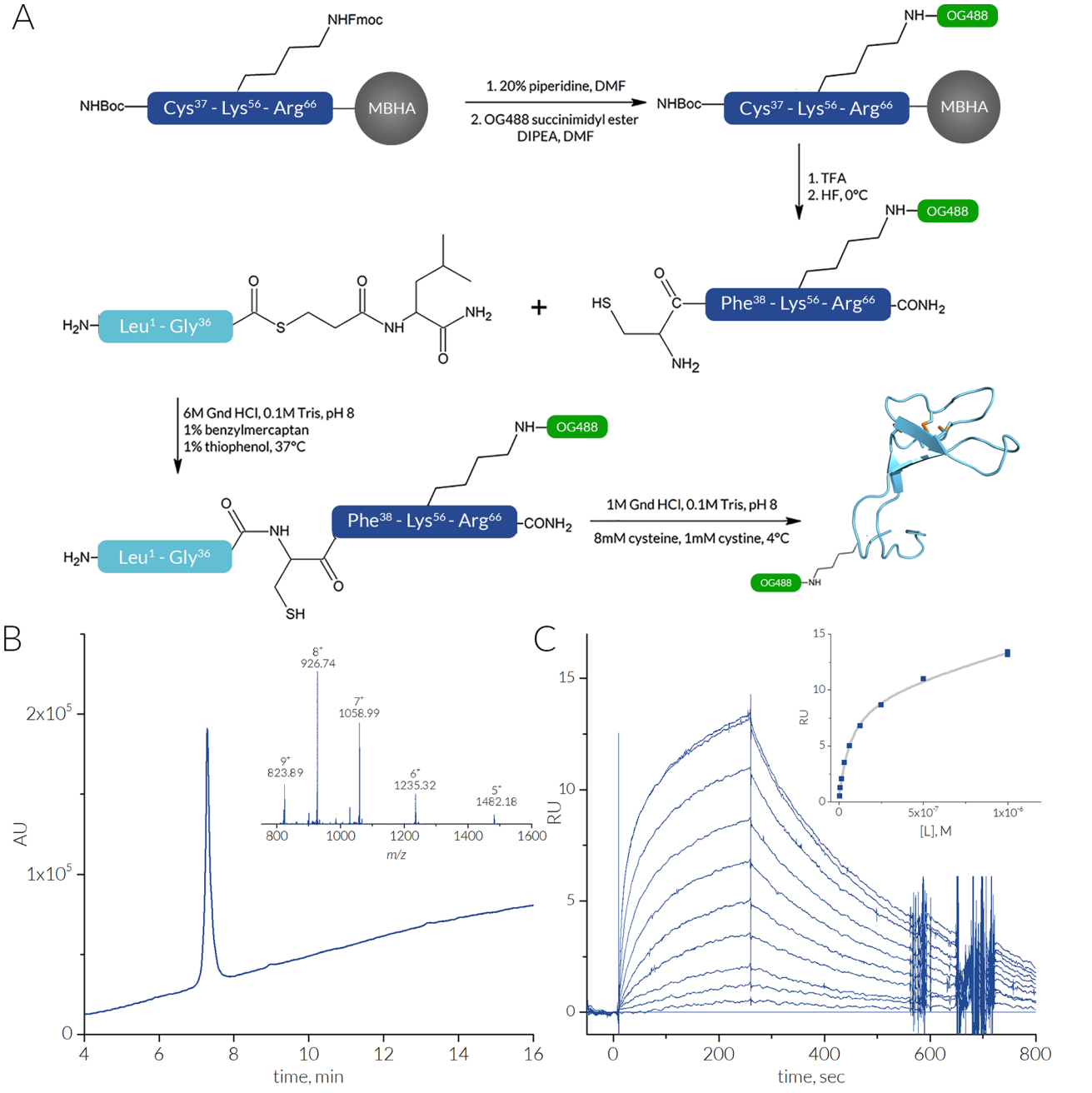

Figure 5. Synthetic Evasin-3 variant uniformly labeled with OG488 retains nM affinity to CXCL1. A. Chemical synthesis of N56K Evasin-3 OG488. B. HPLC track and mass spectrum of purified N56K Evasin-3 OG488. Deconvoluted and calculated mass of $[M + H]^+$ were 7404.16 and 7403.63 Da, respectively. C. Progress and binding curves of N56K Evasin-3 OG488 to CXCL1 immobilized on a streptavidin-coated chip. The apparent K_d value, quantified from the data employing Langmuir-like steady-state affinity model with a linear component, was 68 nM (R_{max} = 9.6, χ^2 = 0.033).

observation most likely indicates the formation of a trimeric [^{15}N,^{13}C] CXCL1/met-Evasin-3/Fondaparinux complex. Thus, Evasin-3 binding to CXCL1 may not be sufficient for CXCL1 removal from GAGs of the cell wall. This assumption opens an opportunity to use Evasin-3 as a probe to detect CXCL1 deposited at the GAGs of the luminal vessel surface and thereby identify inflammation spots in arteries.

To explore this opportunity, we synthesized a conjugate of Evasin-3 and Oregon Green 488 (OG488). A glycosylation site was preferred for labeling to minimize the influence of a bulky fluorophore moiety on Evasin-3 on the affinity to CXCL1 and to retain biological activity. For that reason, the putative N-glycosylation site N56 has been mutated to lysine to allow OG488 coupling through the lysine side chain. This Evasin-3 conjugate was successfully synthesized using Boc-based SPPS and native chemical ligation and named N56K Evasin-3 OG488 (Figure 5A,B). SPR biosensor analysis was used to investigate the affinity of N56K Evasin-3 OG488 to explore the influence of this K56N mutation and fluorophore conjugation on affinity for CXCL1. SPR experiments were performed with synthetic uniformly biotinylated CXCL1 (Figure S5) immobilized on a chip surface coated with streptavidin. Results indicated that Evasin-3 and N56K Evasin-3 OG488 bind CXCL1 in a dose-dependent manner with comparable K_d

https://dx.doi.org/10.1021/acs.bioconjchem.0c00095
Bioconjugate Chem. 2020, 31, 948−955

values of 106 nM and 68 nM, respectively (Figure 5C; Figure S6).

The N56K Evasin-3 OG488 variant was further used for CXCL1 visualization experiments. Previous studies showed that shear stress increased the amount of CXCL1 tethered to EC.[26,27] To explore whether or not N56K Evasin-3 OG488 could bind to CXCL1 tethered on activated ECs, human microvascular endothelial cells (HMVECs) were cultured under 2.0 Pa of shear stress for 72 h to mimic human arterial shear stress. Addition of N56K Evasin-3 OG488 to the flowing medium clearly exhibited binding of N56K Evasin-3 OG488 to shear stress-activated cells, whereas HMVECs cultured under static conditions only showed minimal adherence of N56K Evasin-3 OG488 (Figure 6A,B). Although it has not been

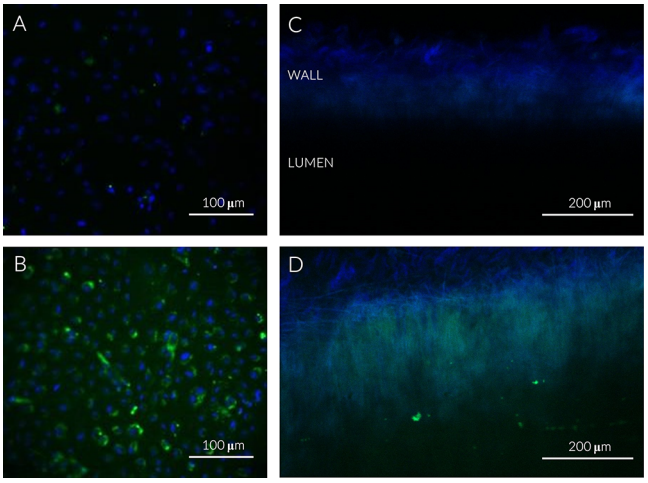

Figure 6. Fluorescently labeled Evasin-3 visualizes CXCL1 in stress-activated HMVECs and LPA-activated murine carotid arteries. HMVECs cultured under static conditions (A) and subjected to 2.0 Pa (20 dyn/cm^2) shear stress for 72 h (B) (green = N56K Evasin-3 OG488, blue = Hoechst). Two-photon laser scanning microscopy of mounted murine carotid arteries without (C) and with LPA treatment for 10 min (D) (green N56K Evasin-3 OG488, blue autofluorescence collagen).

proven experimentally, it is safe to suggest that shear stress triggers expression of several CXC-type chemokines similar to LPA activation. In contrast to CXCL8, CXCL2, -3, -5, and -6 embody conservative positively charged lysines in the region involved in the formation of a CXCL1/Evasin-3/GAG complex (Figure S7A). At least one chemokine, namely, CXCL3, shares the exact pattern of GAG-binding residues with CXCL1. That makes it possible to conclude that N56K Evasin-3 OG488 most likely binds to several CXC-type chemokines deposited on GAGs after shear stress activation of ECs.

To translate these *in vitro* experiments into a more biologically relevant system, LPA-activated endothelium of murine carotid artery was subsequently used in experiments with N56K Evasin-3 OG488. The effect of Evasin-3 on LPA-activated endothelium in whole mounted carotid arteries was studied by TPLSM, as this enables *ex vivo* imaging in vessels. Activation of endothelial cells by perfusion of the carotids with 10 μM LPA resulted in accumulation of N56K Evasin-3 OG488 at the luminal side of the carotid artery, whereas minimal N56K Evasin-3 OG488 adhesion could be observed in control carotids (Figure 6C,D). These results indicate that N56K Evasin-3 OG488 is able to bind to CXC-type chemokines presented on activated endothelium at the luminal vessel surface of affected murine arteries. Comparison of known murine CXC-type chemokines with human CXCL1 (Figure S7B) shows that human and murine CXCL1 share a conservative pattern of GAG-binding residues (H19, K21, K45, R48) with the only exception in the position K49 (E49 in the case of murine CXCL1). Murine CXCL2, -3, and -5 substantially differ from human CXCL1, lacking His and Arg in positions 19 and 48, respectively. Thus, at least one murine chemokine (CXCL1) binds Evasin-3 and GAGs similarly to human CXCL1 and allows for visualization of inflammation in murine arteries.

In summary, we studied binding of Evasin-3 to CXCL1 from the structural standpoint and showed that Evasin-3 can bind CXCL1 deposited on cell wall GAGs. Taking into account that Evasin-3 binds several CXC-type chemokines which share the conservative structure and GAG-binding motifs, Evasin-3 most likely binds several CXC-type chemokines through the same proposed mechanism. Although Evasin-3 is not a selective chemokine binding protein, fluorophore-labeled or even radiolabeled Evasin-3 might be used as a molecular imaging agent for detection of inflamed endothelium, and thus atherosclerotic plaques noninvasively. This hypothesis was proven by imaging of CXC-type chemokines by the fluorescent Evasin-3 conjugate in activated endothelium of HUVEC and whole murine carotid artery. Taking into account that Evasin-3 and its variants could be readily obtained by solid-phase peptide synthesis, Evasin-3 represents an attractive candidate for further development of prospective and more selective imaging agents for cardiovascular diseases.

■ ASSOCIATED CONTENT

Supporting Information

The Supporting Information is available free of charge at https://pubs.acs.org/doi/10.1021/acs.bioconjchem.0c00095.

Experimental procedures, additional NMR and BIACORE analysis results, CXCL1-Biotin synthesis scheme, and characterization (PDF)

■ AUTHOR INFORMATION

Corresponding Author

Ingrid Dijkgraaf − *Department of Biochemistry, Maastricht University, 6229 ER Maastricht, The Netherlands;* Email: i.dijkgraaf@maastrichtuniversity.nl

Authors

Stepan S. Denisov − *Department of Biochemistry, Maastricht University, 6229 ER Maastricht, The Netherlands;* orcid.org/0000-0001-5460-940X

Alexandra C. A. Heinzmann − *Department of Biochemistry, Maastricht University, 6229 ER Maastricht, The Netherlands*

Tanja Vajen − *Department of Biochemistry, Maastricht University, 6229 ER Maastricht, The Netherlands*

Mark H. M. Vries − *Department of Physiology, Maastricht University, 6229 ER Maastricht, The Netherlands*

Remco T. A. Megens − *Department of Biomedical Engineering, Cardiovascular Research Institute Maastricht (CARIM), Maastricht University, 6229 ER Maastricht, The Netherlands; Institute for Cardiovascular Prevention, Ludwig-Maximilians-University, 80336 Munich, Germany*

Dennis Suylen − *Department of Biochemistry, Maastricht University, 6229 ER Maastricht, The Netherlands*

Rory R. Koenen − *Department of Biochemistry, Maastricht University, 6229 ER Maastricht, The Netherlands;* orcid.org/0000-0002-9955-9730
Mark J. Post − *Department of Physiology, Maastricht University, 6229 ER Maastricht, The Netherlands*
Johannes H. Ippel − *Department of Biochemistry, Maastricht University, 6229 ER Maastricht, The Netherlands*
Tilman M. Hackeng − *Department of Biochemistry, Maastricht University, 6229 ER Maastricht, The Netherlands*

Complete contact information is available at: https://pubs.acs.org/10.1021/acs.bioconjchem.0c00095

Notes

The authors declare no competing financial interest.

■ ACKNOWLEDGMENTS

This study was in part performed within the framework of the Center for Translational Molecular Medicine (CTMM), project EMINENCE (grant 01C-204 to M.J.P.; T.M.H.), and in part made possible by The Netherlands Organisation for Scientific Research (NWO; VIDI 723.013.009 and Aspasia 015.010.005 to I.D.) and the Landsteiner Foundation for Blood Transfusion Research (LSBR Nr. 1638, to R.R.K.). Jacques Debets, and Jeroen Hameleers are greatly acknowledged for their assistance with the mouse carotid experiments.

■ REFERENCES

(1) GBD 2013 Mortality and Causes of Death Collaborators (2015) Global, Regional, and National Age-Sex Specific All-Cause and Cause-Specific Mortality for 240 Causes of Death, 1990−2013: A Systematic Analysis for the Global Burden of Disease Study 2013. *Lancet 385* (9963), 117−171.
(2) Sakakura, K., Nakano, M., Otsuka, F., Ladich, E., Kolodgie, F. D., and Virmani, R. (2013) Pathophysiology of Atherosclerosis Plaque Progression. *Heart, Lung Circ. 22* (6), 399−411.
(3) Miller, M. C., and Mayo, K. H. (2017) Chemokines from a Structural Perspective. *Int. J. Mol. Sci. 18* (10), 2088.
(4) Schober, A., Manka, D., Von Hundelshausen, P., Huo, Y., Hanrath, P., Sarembock, I. J., Ley, K., and Weber, C. (2002) Deposition of Platelet RANTES Triggering Monocyte Recruitment Requires P-Selectin and Is Involved in Neointima Formation after Arterial Injury. *Circulation 106* (12), 1523−1529.
(5) Zhou, Z., Subramanian, P., Sevilmis, G., Globke, B., Soehnlein, O., Karshovska, E., Megens, R., Heyll, K., Chun, J., Saulnier-Blache, J. S., et al. (2011) Lipoprotein-Derived Lysophosphatidic Acid Promotes Atherosclerosis by Releasing CXCL1 from the Endothelium. *Cell Metab. 13* (5), 592−600.
(6) Koenen, R. R., and Weber, C. (2011) Chemokines: Established and Novel Targets in Atherosclerosis. *EMBO Mol. Med. 3* (12), 713−725.
(7) Boisvert, W. A., Rose, D. M., Johnson, K. A., Fuentes, M. E., Lira, S. A., Curtiss, L. K., and Terkeltaub, R. A. (2006) Up-Regulated Expression of the CXCR2 Ligand KC/GRO-α in Atherosclerotic Lesions Plays a Central Role in Macrophage Accumulation and Lesion Progression. *Am. J. Pathol. 168* (4), 1385−1395.
(8) Koenen, R. R., von Hundelshausen, P., Nesmelova, I. V., Zernecke, A., Liehn, E. a, Sarabi, A., Kramp, B. K., Piccinini, A. M., Paludan, S. R., Kowalska, M. A., et al. (2009) Disrupting Functional Interactions between Platelet Chemokines Inhibits Atherosclerosis in Hyperlipidemic Mice. *Nat. Med. 15* (1), 97−103.
(9) Weber, C., Meiler, S., Döring, Y., Koch, M., Drechsler, M., Megens, R. T. A., Rowinska, Z., Bidzhekov, K., Fecher, C., Ribechini, E., et al. (2011) CCL17-Expressing Dendritic Cells Drive Atherosclerosis by Restraining Regulatory T Cell Homeostasis in Mice. *J. Clin. Invest. 121* (7), 2898−2910.
(10) Proudfoot, A. E. I., Bonvin, P., and Power, C. A. (2015) Targeting Chemokines: Pathogens Can, Why Can't We? *Cytokine+ 74* (2), 259−267.
(11) Frauenschuh, A., Power, C. a., Deruaz, M., Ferreira, B. R., Silva, J. S., Teixeira, M. M., Dias, J. M., Martin, T., Wells, T. N. C., and Proudfoot, a. E. I. (2007) Molecular Cloning and Characterization of a Highly Selective Chemokine-Binding Protein from the Tick Rhipicephalus Sanguineus. *J. Biol. Chem. 282* (37), 27250−27258.
(12) Hayward, J., Sanchez, J., Perry, A., Huang, C., Rodriguez Valle, M., Canals, M., Payne, R. J., and Stone, M. J. (2017) Ticks from Diverse Genera Encode Chemokine-Inhibitory Evasin Proteins. *J. Biol. Chem. 292* (38), 15670−15680.
(13) Lee, A. W., Deruaz, M., Lynch, C., Davies, G., Singh, K., Alenazi, Y., Eaton, J. R. O., Kawamura, A., Shaw, J., Proudfoot, A. E. I., et al. (2019) A Knottin Scaffold Directs the CXC-Chemokine-Binding Specificity of Tick Evasins. *J. Biol. Chem. 294* (29), 11199−11212.
(14) Copin, J.-C., da Silva, R. F., Fraga-Silva, R. A., Capettini, L., Quintao, S., Lenglet, S., Pelli, G., Galan, K., Burger, F., Braunersreuther, V., et al. (2013) Treatment with Evasin-3 Reduces Atherosclerotic Vulnerability for Ischemic Stroke, but Not Brain Injury in Mice. *J. Cereb. Blood Flow Metab. 33* (4), 490−498.
(15) Weber, K. S. C., Von Hundelshausen, P., Clark-Lewis, I., Weber, P. C., and Weber, C. (1999) Differential Immobilization and Hierarchical Involvement of Chemokines in Monocyte Arrest and Transmigration on Inflamed Endothelium in Shear Flow. *Eur. J. Immunol. 29* (2), 700−712.
(16) Huo, Y., Weber, C., Forlow, S. B., Sperandio, M., Thatte, J., Mack, M., Jung, S., Littman, D. R., and Ley, K. (2001) The Chemokine KC, but Not Monocyte Chemoattractant Protein-1, Triggers Monocyte Arrest on Early Atherosclerotic Endothelium. *J. Clin. Invest. 108* (9), 1307−1314.
(17) Zernecke, A., Bot, I., Djalali-Talab, Y., Shagdarsuren, E., Bidzhekov, K., Meiler, S., Krohn, R., Schober, A., Sperandio, M., Soehnlein, O., et al. (2008) Protective Role of CXC Receptor 4/CXC Ligand 12 Unveils the Importance of Neutrophils in Atherosclerosis. *Circ. Res. 102* (2), 209−217.
(18) Soehnlein, O., Zernecke, A., and Weber, C. (2009) Neutrophils Launch Monocyte Extravasation by Release of Granule Proteins. *Thromb. Haemostasis 102* (2), 198−205.
(19) Montecucco, F., Lenglet, S., Gayet-Ageron, A., Bertolotto, M., Pelli, G., Palombo, D., Pane, B., Spinella, G., Steffens, S., Raffaghello, L., et al. (2010) Systemic and Intraplaque Mediators of Inflammation Are Increased in Patients Symptomatic for Ischemic Stroke. *Stroke 41* (7), 1394−1404.
(20) Déruaz, M., Frauenschuh, A., Alessandri, A. L., Dias, J. M., Coelho, F. M., Russo, R. C., Ferreira, B. R., Graham, G. J., Shaw, J. P., Wells, T. N. C., et al. (2008) Ticks Produce Highly Selective Chemokine Binding Proteins with Antiinflammatory Activity. *J. Exp. Med. 205* (9), 2019−2031.
(21) Denisov, S. S., Ippel, J. H., Heinzmann, A. C. A., Koenen, R. R., Ortega-Gomez, A., Soehnlein, O., Hackeng, T. M., and Dijkgraaf, I. (2019) Tick Saliva Protein Evasin-3 Modulates Chemotaxis by Disrupting CXCL8 Interactions with Glycosaminoglycans and CXCR2. *J. Biol. Chem. 294* (33), 12370−12379.
(22) Poluri, K. M., Joseph, P. R. B., Sawant, K. V., and Rajarathnam, K. (2013) Molecular Basis of Glycosaminoglycan Heparin Binding to the Chemokine CXCL1 Dimer. *J. Biol. Chem. 288*, 25143−25153.
(23) Joseph, P. R. B., Mosier, P. D., Desai, U. R., and Rajarathnam, K. (2015) Solution NMR Characterization of Chemokine CXCL8/IL-8 Monomer and Dimer Binding to Glycosaminoglycans: Structural Plasticity Mediates Differential Binding Interactions. *Biochem. J. 472* (1), 121−133.
(24) Sepuru, K. M., and Rajarathnam, K. (2016) CXCL1/MGSA Is a Novel Glycosaminoglycan (GAG)-Binding Chemokine. *J. Biol. Chem. 291* (8), 4247−4255.
(25) Sepuru, K. M., and Rajarathnam, K. (2019) Structural Basis of Chemokine Interactions with Heparan Sulfate, Chondroitin Sulfate, and Dermatan Sulfate. *J. Biol. Chem. 294* (43), 15650−15661.

(26) Hagiwara, H., Mitsumata, M., Yamane, T., Jin, X., and Yoshida, Y. (1998) Laminar Shear Stress-Induced GRO MRNA and Protein Expression in Endothelial Cells. *Circulation 98* (23), 2584−2590.
(27) Vries, M. H. M., Wagenaar, A., Verbruggen, S. E. L., Molin, D. G. M., and Post, M. J. (2015) CXCL1 Promotes Arteriogenesis through Enhanced Monocyte Recruitment into the Peri-Collateral Space. *Angiogenesis 18* (2), 163−171.

https://dx.doi.org/10.1021/acs.bioconjchem.0c00095
Bioconjugate Chem. 2020, 31, 948−955